Impact of an initial random magnetic field on the evolution of two-dimensional shearless mixing layers

Mahzad Chitsaz and Mani Fathali*
Department of Aerospace Engineering, K. N. Toosi University of Technology, Tehran, Iran

(Received 18 April 2019; published 14 October 2019)

The impact of an initial random magnetic field on the temporal evolution of a two-dimensional incompressible turbulent shearless mixing layer is investigated using direct numerical simulation. Different intensities of the initial random magnetic field are imposed with uniform probability distribution on an identical flow field. The initial flow field condition is the turbulent shearless mixing layer with different kinetic energy ratio ($E_H/E_L = 6.7$) and identical integral length scale. Simulations are carried out in a moderate magnetic Reynolds number, which causes a two-way interaction between the velocity and magnetic fields. In order to analyze the effect of the initial random magnetic field on the mixing characteristics, the intermittency inside the mixing layer and the mixing evolution parameters are investigated. It is found that with small initial magnetic field intensity, the intermittency in both large and small scales are larger than those values in hydrodynamic flow. However, increasing the intensity of the initial magnetic field reduces the intermittency in the mixing region to lower values compared to the hydrodynamic flow. The mixing layer growth rate and the mixing efficiency both show reduction by increasing the initial magnetic field intensity, which is attributed to the reduction of the averaged Reynolds number of both homogenous isotropic turbulent regions due to the suppressing effect of the Lorentz force on the velocity fields of these regions.

DOI: 10.1103/PhysRevE.100.043106

I. INTRODUCTION

Turbulent mixing is present in many natural astrophysical and geophysical phenomena as well as in industrial and technical applications. The simplest turbulent mixing case occurs where there are two fluids with similar properties stretch and fold throughout the domain [1]. However, the mixing process generally occurs in more complicated situations, in which fluid dynamics or its properties are affected by other parameters such as drag forces and chemical reactions. Therefore, due to the diversity and complexity of the mixing processes, it is important to investigate the mixing quality in various types of flow and conditions under which mixing occurs.

Since shearless mixing layer represents one of the simplest inhomogeneous flows, it can be considered as one of the most appropriate candidates to investigate turbulent mixing behaviors [2]. The shearless mixing layer is produced in a decaying grid turbulence in which the mean velocity is constant throughout the flow field but two different homogenous isotropic turbulent (HIT) regions are formed on either side of the stream [3]. As the flow evolves, the energetic eddies penetrate from one HIT field into another and form an anisotropic mixing region [4]. In this flow, due to the absence of the mean velocity gradient across the layer, there is no mechanism for production of the turbulent kinetic energy. Therefore, the shearless mixing layer serves as a useful benchmark flow to investigate the fundamental aspects of a mixing process that is exclusively originated from fluctuating pressure and velocity fields [2,5].

Over the last three decades, several theoretical and experimental research works and developments have been performed on the two-dimensional (2D) and three-dimensional (3D) shearless mixing layers, which have provided a strong foundation to study mixing processes. The early study of shearless turbulent mixing was carried out experimentally by Gilbert [3]. In his experiment, the turbulent kinetic energy gradient was produced using a passive grid with two distinct scales. Gilbert's study focused mainly on the downstream evolution of the mixing layer width. Therefore, no significant levels of the intermittency and departure from the Gaussian statistics in the velocity were observed. In a more detailed experimental study by Veeravalli and Warhaft [4], the mixing evolution in the shearless mixing layer with both turbulent kinetic energy and length scale gradients was investigated. Unlike the results of Gilbert's study, this research represented significant deviations from Gaussian statistics or intermittency by examining the velocity skewness and flatness coefficients. Moreover, shifting the locations of the skewness and flatness maxima toward the low-kinetic energy region revealed that mixing occurs by penetration of the high-kinetic energy turbulent eddies into the low-energy region.

Later, several numerical investigations were performed which all confirmed the results obtained by Veeravalli and Warhaft. Tordella and Iovieno showed that the intermittency level and the growth of the mixing region increase when the turbulent kinetic energy and length scale gradients are concordant [6]. Later investigations [2,7] showed that

*mfathali@kntu.ac.ir

a sufficient condition for emergence of the intermittency is the presence of the turbulent energy or the length scale gradients.

Using both numerical and experimental approaches, Kang and Meneveau [8] found that much of the departure from Gaussian statistics originates from the large-scale motions in high-Reynolds number flows. Nevertheless, Tordella and Iovieno [9] showed that decaying shearless turbulent mixing leads to a significant level of the small-scale anisotropy and intermittency, which are identified by the normalized third- and fourth-order one-point moments of the longitudinal velocity derivative.

In another numerical study, Iovieno *et al.* investigated the mixing of passive scalars in 2D and 3D shearless mixing layers [10]. In this research, they showed that the evolutions of 2D and 3D shearless turbulent mixing are qualitatively and quantitatively different. In a more recent study, Fathali and Khoshnami [5] focused on the sensitivity of a 2D shearless mixing layer evolution to the variations of the length scale and the turbulent kinetic energy ratios. It was found that the turbulent kinetic energy was the most influential parameter on the variability of mixing evolution. In addition, it was indicated that dependency of the mixing intermittency and energy transfer mechanisms on the length scale and turbulent kinetic energy ratios is different from that of the mixing growth rate and the mixing efficiency.

All the above mentioned studies were conducted on single-phase and nonreacting flows with no imposed external forces. In these kind of flows, the turbulent flow dynamic is affected only by kinetic energy or the length scale gradients, which leads to mixing evolution. However, in many real situations, turbulent mixing occurs in a more complicated flow, where its dynamics depend on some other factors (e.g., polymers, magnetic force, and multiphase flows). Moreover, there are some fluids whose properties change during the mixing process via other phenomena (e.g., combustion, detonations, and thermonuclear supernova explosions) [11]. Although mixing in such flows is more often accompanied by shear, some research has investigated the mixing of these flows in shearless mixing layer conditions to eliminate the complexities of the shear force effects [12–15].

Magnetohydrodynamic (MHD) mixing is one of the most complex flows that are commonly observed in many natural phenomena and industrial applications, such as astronomy, geophysics, and metallurgy. The dynamics of MHD flows is highly affected by the coupling between velocity and magnetic fields, which are described by combination of the Navier-Stokes (N-S) and the Maxwell equations [16]. This coupling causes the mixing processes in MHD flows to be more complicated compared to the hydrodynamic (HD) turbulent flows.

Most research on the MHD mixing layer has been conducted using shear flow conditions in which development of the Kelvin-Helmholtz instability leads to the energy transport, dissipation, and mixing of fluids. Therefore, most of these focused on interactions of Kelvin-Helmholtz instability and the external magnetic field [17–19], as well as their impact on some phenomena such as ion mixing [20,21], magnetic reconnection [22,23], and passive scalar and particle dispersion [24–26].

In contrast to the MHD shear mixing layer, there are very limited reported studies on the MHD shearless mixing layer. In these research works, the applicability of the large eddy simulation method for predicting different aspects of the MHD shearless mixing layer with random initial magnetic field are explored [27,28].

The study of the MHD shearless mixing layer evolution is motivated by the fact that the intermittent mixing and departure from the Gaussian statistics, originated from the turbulence-turbulence interactions, can be significantly affected by the presence of the magnetic field, and the shearless mixing layer is one of the most appropriate flow field configurations for investigating these processes. In addition, study of the MHD shearless mixing layer is beneficial for understanding the impact of the magnetic field on the development of the magnetohydrodynamic turbulence intermittency, which is commonly observed in many geophysical and astrophysical problems [27,29].

Although 2D and 3D MHD turbulence show similarities in certain respects, e.g., direct cascades of the turbulent kinetic energy and helicity [30], there are also significant differences. Indeed, 2D MHD turbulence shows more intermittent spatial distribution compared to the 3D counterpart [31]. Therefore, it is expected that the 2D and 3D MHD shearless mixing layers show nontrivially different dynamics.

Notably, despite these differences between dynamics of the 2D and 3D MHD shearless mixing layers, all the above-mentioned research has been carried out on the 3D MHD shearless mixing layer. To the best of the authors' knowledge, there is no previous report on the 2D MHD shearless mixing layer.

Accordingly, this research aims at identifying the impact of the initial random magnetic field on the (1) intermittency and departure from Gaussian statistics inside the mixing region and (2) the mixing process in a 2D MHD shearless mixing layer, using the DNS approach.

Indeed, the Alfvén timescale, as the relevant nonlinear timescale, is closely related to the magnitude of the large-scale magnetic field. A random magnetic field can have nontrivial effect on the spectral distribution of the kinetic energy, resulting in the Kolmogorov-like MHD turbulence [32,33]. Therefore, from the theoretical point of view, the response of the 2D turbulent mixing to the additional degrees of freedom, i.e., random magnetic field, is very pertinent to the general understanding of the MHD turbulent mixing. In terms of astrophysical implications, the galactic dynamo is influenced by the large-scale random magnetic fields.

This paper is organized as follows: In Sec. II the governing equations, flow field configuration, and its initialization are briefly explained. Next, in Sec. III the changes of statistics and mixing properties under various initial random magnetic fields are analyzed and presented. Finally, conclusions are summarized in Sec. IV.

II. INITIAL CONDITIONS AND METHOD OF SOLUTION

In this research, the pseudospectral method is used for direct numerical simulation (DNS) of an incompressible 2D shearless mixing layer evolution with initial random magnetic field. To enforce the periodicity, as a requirement of this

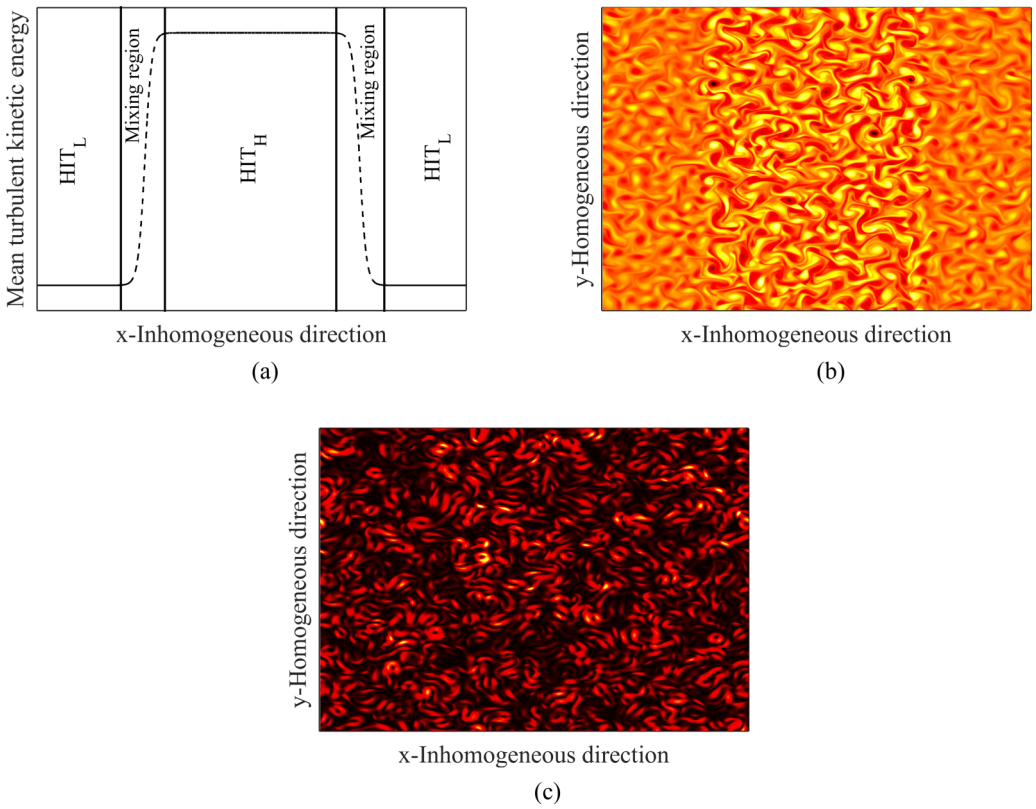

FIG. 1. (a) Graphical representation of the initial flow field configuration consisting of two shearless mixing layers. Dashed line presents the turbulent kinetic energy level of different regions. (b) Initial velocity field; (c) initial magnetic field.

numerical method, two shearless mixing layers are considered side by side, which perform the reverse transition compared to each other [5,34]. This also improves the statistics of results through average data gathered from the two mixing layers in each DNS [34]. The shearless mixing layer consists of two HIT regions with different turbulent kinetic energy intensities that are in contact and interact through a thin transition layer [5]. The initial flow field configuration is shown in Fig. 1(a), where $\mathrm{HIT_H}$ and $\mathrm{HIT_L}$ represent high- and low-energy HIT regions, respectively [see Fig. 1(b)]. This initial mixing layer flow can be described as [5]

$$\omega(x,y) = [1 - f(x)]^{\frac{1}{2}}\omega_L(x,y) + f(x)^{\frac{1}{2}}\omega_H(x,y), \quad (1)$$

where $\omega_H(x,y)$ and $\omega_L(x,y)$ are the vorticity fields of HIT_H and HIT_L, respectively. The function $f(x)$ is [5]

$$f(x) = \frac{1}{2}\left[1 + p(0)p\left(\frac{L}{4}\right)p\left(\frac{3L}{4}\right)\right],$$
$$p(\zeta) = \tanh\left(c\frac{x-\zeta}{L}\right), \quad (2)$$

where L is the size of the computational domain and is equal to 2π. The dimensionless constant c determines the initial layer thickness and is set to 125 to ensure that layer width and the smallest flow field integral length scale ($\frac{L}{150}$) are in the same order [5]. Each HIT vorticity field is generated in the Fourier space with the following amplitudes:

$$\hat{\omega}(k_x, k_y, 0) = \left[\frac{k^2 E_s(k,0)}{\pi}\right]^{\frac{1}{2}} \exp(i\theta), \quad (3)$$

where $i = \sqrt{-1}$, θ is the random phase, which is expressed by $\theta \in [0, 2\pi]$ with uniform PDF, and $E_s(k,0)$ is the initial energy spectrum [5]:

$$E_s(k,0) = \frac{1}{k_p}\left(\frac{k}{k_p}\right)^7 \exp\left[-3.5\left(\frac{k}{k_p}\right)^2\right], \quad (4)$$

where $k^2 = {k_x}^2 + {k_y}^2$ is the spectral radius [35]. k_p is the peak wave number, which is related to the length scale in 2D turbulence with the following expression [5,35,36]:

$$\ell = \left[\frac{\int_0^\infty E_s(k)\,dk}{\int_0^\infty k^2 E_s(k)\,dk}\right]^{\frac{1}{2}} = \sqrt{\frac{7}{8}}{k_p}^{-1}. \quad (5)$$

There are different interpretations of this length scale in Refs. [35–37]. In Ref. [35] the length scale ℓ is considered as the microscale length scale. On the contrary, in Refs. [36,37] this length scale is attributed to the integral length scale according to the definition given in Ref. [38], $L_{\mathrm{int}} = \int_0^\infty k^{-1}E_s(k)\,dk / \int_0^\infty E_s(k)\,dk$. However, it can be shown that for the energy spectrum which is defined in Eq. (4), the length scale ℓ and the integral length scale L_{int} are in the same order, i.e., $L_{\mathrm{int}} = 1.13\ell$ [5].

Each HIT velocity field needs to evolve by a freely decaying simulation until a well-developed isotropic energy spectrum among different Fourier modes is established. Since the integral length scale increases during the flow field evolution, to restore the desired length scale ℓ, the peak wave number k_p in the initial energy spectrum [Eq. (4)] is set as

TABLE I. Details of different initial conditions.

Initial magnetic field intensities ($\mathcal{B}$)	0, 0.05, 0.1, 0.15,
(cont.)	0.2, 0.25, 0.5
Magnetic Reynolds number of $\mathrm{HIT_H}$(Re_{m_H})	20
Reynolds number of $\mathrm{HIT_H}$ (Re_H)	60
Kinematic viscosity (ν)	0.005
Integral length scale (ℓ)	0.042
Turbulen kinetic energy ratio ($E_r = \frac{E_H}{E_L}$)	6.7
Integral length scale ratio ($\ell_r = \frac{\ell_H}{\ell_L}$)	1

0.9ℓ [5]. Depending on the desired integral length scale, this adjustment evolution approximately endures between 5τ and 10τ, where $\tau = \ell/\sqrt{E}$ is the eddy turnover time and E is the turbulent kinetic energy. Subsequently, the Fourier amplitudes of the time-evolved HIT field are rescaled in such a way that the flow field turbulent kinetic energy is adapted to its prescribed initial level.

The initial magnetic field is considered as a random seed with uniform zero-mean probability distribution, which is imposed on the entire flow field [see Fig. 1(c)]. The same procedure of HIT velocity field initialization is used to generate the initial random magnetic field. The integral length scales of the magnetic and velocity fields are identical. Furthermore, the level of magnetic energy (E_m) is determined based on the turbulent kinetic energy of $\mathrm{HIT_H}$, E_H, as

$$E_m = \mathcal{B}E_H, \tag{6}$$

where $\mathcal{B}$ is a dimensionless parameter, which indicates the intensity of the magnetic field.

A summary of the initial conditions used in this numerical research are listed in Table I. In all cases the initial shearless mixing layer flow field is kept constant while the initial magnetic field intensity, $\mathcal{B}$, takes different values as presented in Table I. In this table, only the Reynolds number and magnetic Reynolds number of the $\mathrm{HIT_H}$, Re_H and Re_{m_H}, are presented. Generally, the magnetic Reynolds number, Re_m, measures the relative magnitudes of induced and dissipated magnetic fields and is defined as [39]

$$\mathrm{Re}_m = \frac{u_{rms}\ell}{\lambda}, \tag{7}$$

where λ is the magnetic diffusivity, u_{rms} is the square root of the turbulent kinetic energy $\sqrt{E}$, and ℓ is the flow field integral length scale. If Re_m is moderate or large ($\mathrm{Re}_m \gg 1$), there is a strong two-way interaction between the velocity and magnetic fields. On the other hand, when Re_m is small ($\mathrm{Re}_m \ll 1$), the effect of the velocity field on the magnetic field induction is negligible, whereas the imposed magnetic field suppresses the turbulent activity [39]. In this research, in order to simultaneously examine the mutual interaction of velocity and magnetic fields besides the viscous and Ohmic dissipations, both kinetic and magnetic Reynolds numbers are considered in moderate ranges (see Table I) [26].

Furthermore, regarding the values of Re and Re_m in Table I, the magnetic Prandtl number (which is defined as ratio of Re_m to Re) is about 0.33. Although this magnetic Prandtl number is far from those of liquid metals or astrophysical plasmas, it can still provide valuable information on the inertial range properties of the MHD flows [40,41].

Moreover, a passive scalar is also introduced in the flow field in order to investigate its dynamics under the influence of the initial random magnetic field. The passive scalars are distributed in the $\mathrm{HIT_H}$ and $\mathrm{HIT_L}$ regions with an initial uniform concentration of $Z = 1$ and $Z = 0$, respectively. Furthermore, the passive scalar concentration of the mixing region is matched through the following equation [5]:

$$Z(x, y) = f(x)^{\frac{1}{2}}\omega_H(x, y), \tag{8}$$

where $f(x)$ was introduced in Eq. (2).

The evolution of incompressible MHD turbulence can be determined by solving the governing equations of MHD, which are a combination of a reduced form of Maxwell's equations and the N-S equations [39]. In this case, the N-S equations are used in vorticity formulation to eliminate the pressure variable:

$$\frac{\partial\vec{\omega}}{\partial t} = \vec{\nabla}\times(\vec{u}\times\vec{\omega} - \vec{b}\times\vec{J}) + \nu\nabla^2\vec{\omega}, \tag{9}$$

$$\frac{\partial\vec{b}}{\partial t} = \vec{\nabla}\times(\vec{u}\times\vec{b}) + \lambda\nabla^2\vec{b}, \tag{10}$$

$$\vec{\nabla}\cdot\vec{u} = 0, \tag{11}$$

$$\vec{\nabla}\cdot\vec{b} = 0, \tag{12}$$

where

$$\vec{\omega} = \vec{\nabla}\times\vec{u}, \tag{13}$$

$$\vec{J} = \vec{\nabla}\times\vec{b}, \tag{14}$$

$$\text{Lorentz force} = \vec{J}\times\vec{b}, \tag{15}$$

where ν is the kinematic viscosity and $\vec{b}$ is the magnetic field, which is denoted in Alfvénic units and is measured in the same units as the bulk velocity. Furthermore, the evolution of the passive scalar is defined as

$$\frac{\partial Z}{\partial t} + \vec{u}\cdot\vec{\nabla}Z = D_Z\nabla^2 Z, \tag{16}$$

where D_Z is the molecular diffusivity and is defined as

$$D_Z = \frac{\nu}{\mathrm{Sc}}, \tag{17}$$

where Sc is the Schmidt number and is set as $\mathrm{Sc} = 1$.

All cases are simulated by a classical pseudospectral method at the N^2 equally spaced (collocation) points, $N = 600$. The nonlinear terms are calculated in physical space and dealiased using the 2/3 rule [42]. Also, the time integration is performed using a low-storage, fourth-order Runge-Kutta method with the coefficients of $\alpha_i = \{1/4, 1/3, 1/2, 1\}$, and the total integration time for all simulations is considered as $t = 25\tau$.

III. RESULTS AND DISCUSSIONS

To observe the effect of initial magnetic field intensity on the mixing process of flow field, the evolution of vorticity field and scalars is investigated. Figure 2 visualizes both vorticity

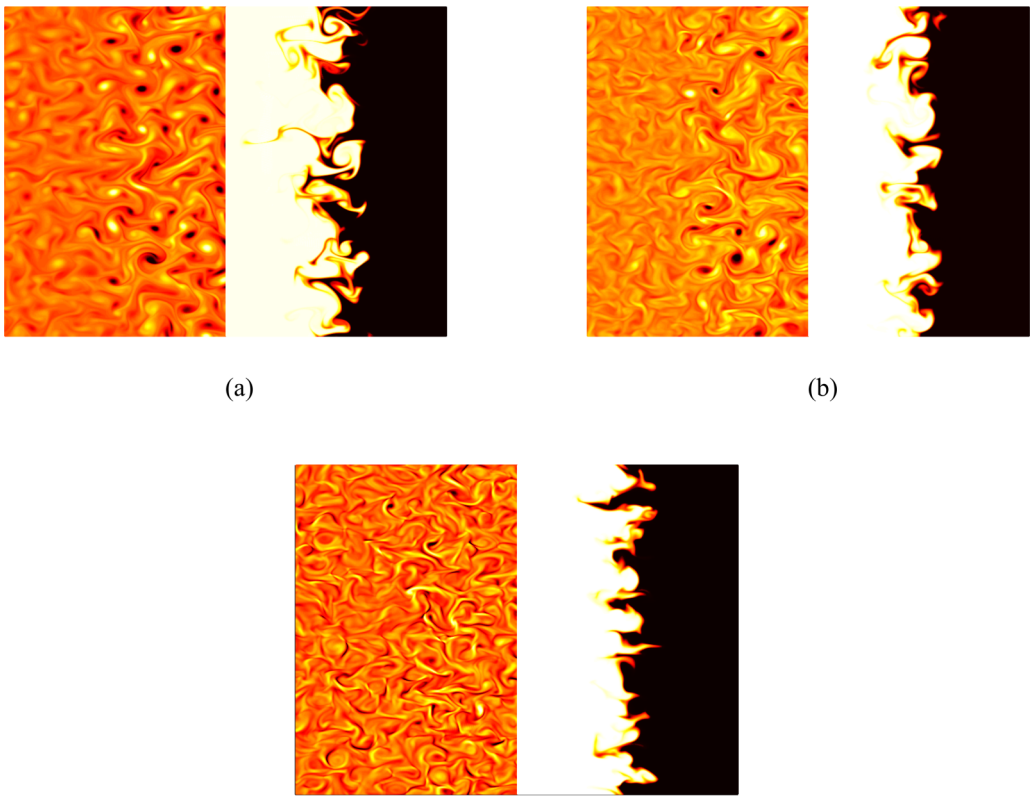

(a) (b)

(c)

FIG. 2. Vorticity-scalar snapshots of shearless mixing layers with imposed magnetic field intensity (a) $\mathcal{B} = 0$, (b) $\mathcal{B} = 0.1$, and (c) $\mathcal{B} = 0.5$ under the same flow initial condition, at $t = 25\tau$. In each snapshot, the scalar and vorticity fields are located at the right and left side of the images, respectively. The horizontal and vertical axes show the inhomogeneous and the homogeneous directions, respectively.

ω and scalar concentration Z fields at $t = 25\tau$, corresponding to three different magnetic field magnitudes, $\mathcal{B}$, imposed on the same flow initial condition. In each snapshot, the vorticity field and scalar concentration are shown on the left and right side of the images, respectively.

The overall evolution of the HD ($\mathcal{B} = 0$) mixing layer in Fig. 2(a) shows that, due to the random motions of the coherent vortical structures, eddies penetrate intermittently from the $\mathrm{HIT_H}$ into the $\mathrm{HIT_L}$ field. These penetrations form a layer between two adjacent HIT fields, in which interface structures of passive scalars are deformed into engulfed regions with intricate and corrugated small-scale structures. The vortical penetration inside the mixing layer causes velocity statistics to be non-Gaussian and highly intermittent. This will be discussed in more detail in Sec. III A.

By comparing Figs. 2(b) and 2(c) with Fig. 2(a), it is observed that the wavy appearance of interface structures of scalars diminishes by increasing $\mathcal{B}$. This indicates less penetration of the passive scalars from one HIT region into the adjacent one. Moreover, it is found that the mixing layer is suppressed further with increasing $\mathcal{B}$, so that in Fig. 2(c) the evolved vorticity field looks isotropic. This suppression occurs due to the effect of the Lorentz force on the flow field such that $\mathrm{HIT_H}$ decays much faster than $\mathrm{HIT_L}$. The impacts of the magnetic and velocity field interactions on mixing layer growth are investigated with details in Sec. III B.

A. Effect of magnetic field on intermittency and anisotropy of the mixing layer

In this section, the anisotropy and intermittency inside the mixing layer are measured to quantify the impact of the initial magnetic field on the turbulent structures of the mixing layer. Under this condition, the mixing layer anisotropies occur due to the intermittent penetration of energetic eddies from the high-energy region into the low-energy region. Hence, the maxima of skewness and kurtosis are considered as the principal indicators to measure the intermittency and departure from Gaussianity inside the mixing layer [9].

In this research, maximum values of velocity skewness, $S_u^{\max}$, and velocity derivative skewness, $S_{u_x}^{\max}$, in the inhomogeneous direction, x, are used to explore the effect of initial magnetic field on the intermittency and anisotropy in both large- and small-scale flow field structures across the mixing layer. The skewness values of velocity and velocity derivative are defined as [43]

$$S_u = \frac{\overline{u^3}}{(\overline{u^2})^{\frac{3}{2}}}, \quad S_{u_x} = \frac{\overline{{u_x}^3}}{(\overline{{u_x}^2})^{\frac{3}{2}}}, \tag{18}$$

where u and u_x are velocity and the velocity derivative in the inhomogeneous direction, x, respectively.

To obtain fully converged statistical results for each test case, 100 independent and statistically identical realizations

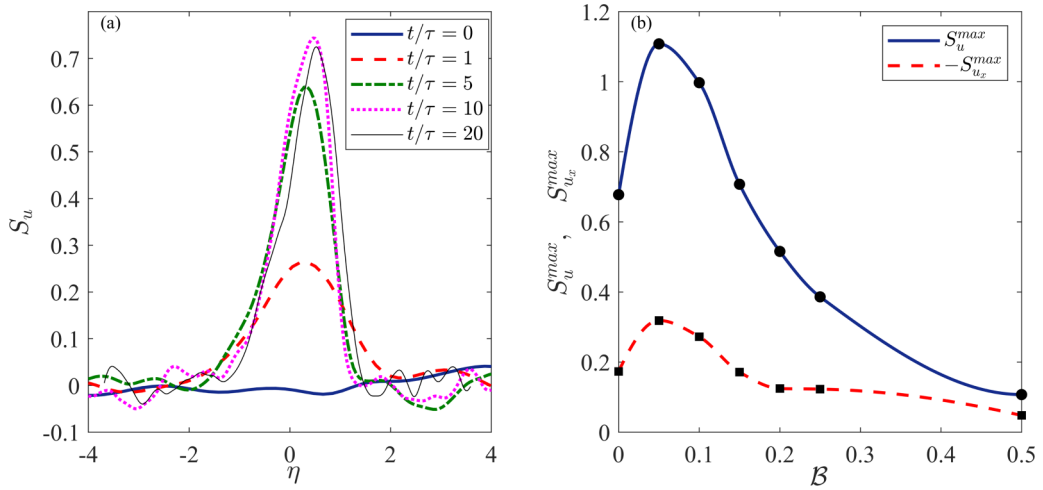

FIG. 3. (a) Spatial distribution of the inhomogeneous velocity skewness of the HD mixing layer ($\mathcal{B} = 0$). The $\mathrm{HIT_H}$ and $\mathrm{HIT_L}$ regions are located at $\eta < 0$ and $\eta > 0$. (b) $S_u^{\max}$(—) and ($S_{u_x}^{\max}$) (– –) variations in inhomogeneous direction at $t = 25\tau$ as a function of $\mathcal{B}$.

are generated using DNS. Figure 3(a) shows the velocity skewness in the mixing layer of hydrodynamic flow ($\mathcal{B} = 0$) at different times. In this figure, the $\mathrm{HIT_H}$ and $\mathrm{HIT_L}$ regions are located at $\eta < 0$ and $\eta > 0$, respectively, where η is the inhomogeneous axis normalized by the thickness of the mixing layer Δ, $\eta = x/\Delta$. The thickness Δ is equal to the distance between the scalar points with the condition $0.25 \leqslant Z(x,t) \leqslant 0.75$. As shown in Fig. 3(a), the S_u in both $\mathrm{HIT_H}$ and $\mathrm{HIT_L}$ regions is zero, which indicates Gaussianity, whereas the positive value of skewness of the inhomogeneous velocity component in the mixing layer shows that the energetic eddies penetrate intermittently across the mixing layer from $\mathrm{HIT_H}$ toward $\mathrm{HIT_L}$ [5]. Likewise, the simulation of MHD flows for different values of $\mathcal{B}$ shows an almost similar trend for S_u in the inhomogeneous direction of the mixing region (results are not shown).

To investigate the effect of the initial magnetic field on the development of intermittency inside the mixing layer, $S_u^{\max}$ and $S_{u_x}^{\max}$ at $t = 25\tau$ are presented as a function of $\mathcal{B}$ in Fig. 3(b). It is observed that, with small initial magnetic fields ($\mathcal{B} \leqslant 0.15$), $S_u^{\max}$, $S_{u_x}^{\max}$, and consequently the mixing layer intermittency are larger compared to the values in HD flow ($\mathcal{B} = 0$). Nonetheless, the descending rate of $S_u^{\max}$ and $S_{u_x}^{\max}$ in MHD flows indicates the reduction of both large- and small-scale intermittency by increasing $\mathcal{B}$. Besides, it is seen that $S_u^{\max}$ decreases faster than $S_{u_x}^{\max}$. Therefore, it is concluded that under the conditions considered in this study, the large-scale eddies are more influenced by the magnetic field compared to the small-scale structures.

Considering that the level of intermittency is related to the effective turbulent kinetic energy ratio of two interacting HIT regions, $E_r(t) = E_H(t)/E_L(t)$, and the integral length scale ratio, $\ell_r(t) = \ell_H(t)/\ell_L(t)$ [5,9], the impact of initial magnetic field on these parameters is investigated. Figure 4(a) illustrates the time evolution of E_r over the range of $\mathcal{B}$. It is observed that, with $\mathcal{B} < 0.15$, E_r grows faster than with $\mathcal{B} = 0$. The same trend is seen with $\mathcal{B} = 0.15$ at the well-developed stage ($t > 10\tau$). In these cases, the Lorentz force induced by the magnetic field suppresses the velocity field in both HIT regions, with a larger descending rate of energy in

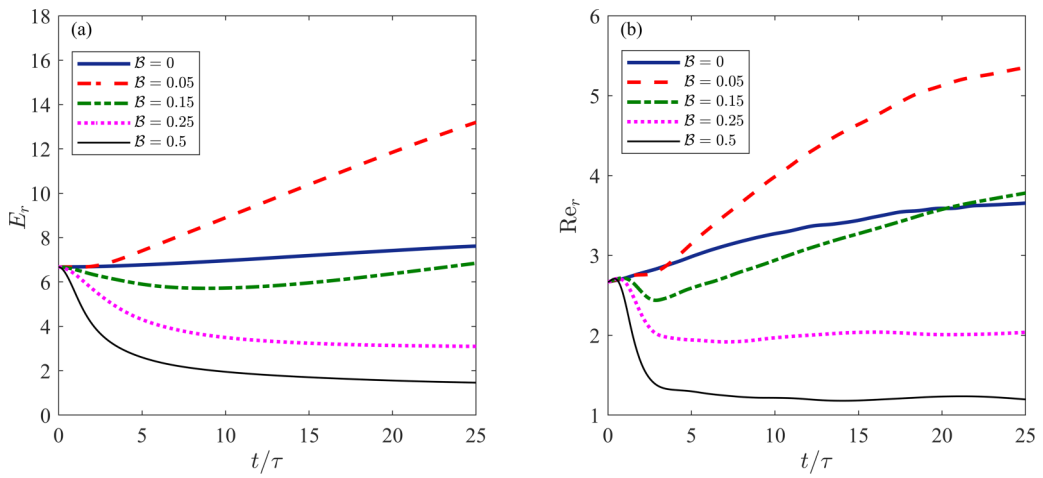

FIG. 4. (a) Time evolution of effective turbulent kinetic energy ratio [$E_r(t) = E_H(t)/E_L(t)$] for different values of $\mathcal{B}$. (b) Time evolution of Reynolds number ratio ($\mathrm{Re}_r = \mathrm{Re}_H/\mathrm{Re}_L$) for different intensities of $\mathcal{B}$.

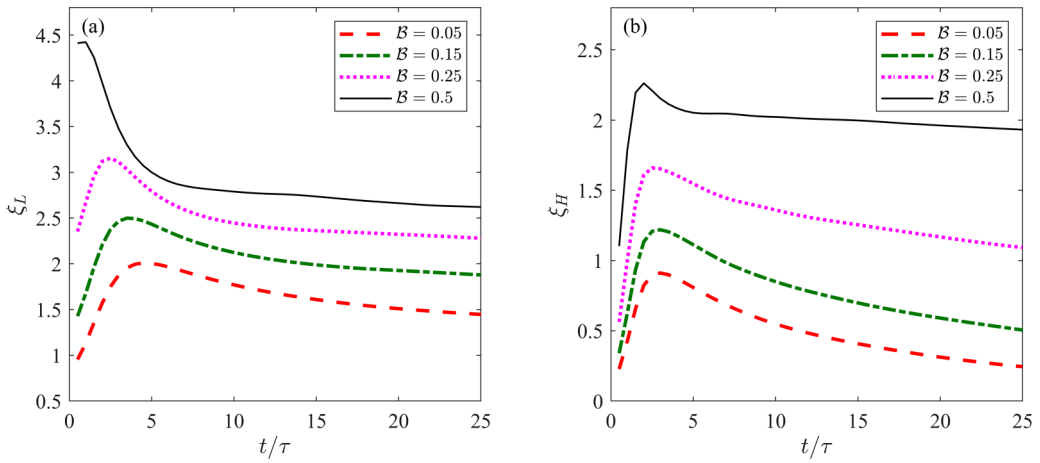

FIG. 5. Time evolution of ξ in (a) $\mathrm{HIT_L}$ (ξ_L) and (b) $\mathrm{HIT_H}$ (ξ_H), for different intensities of $\mathcal{B}$.

$\mathrm{HIT_L}$, $\dot{E}_H < \dot{E}_L$ (this will be discussed shortly). The growth of E_r results in further penetration of energetic eddies in the mixing layer. Therefore, a larger value of $S_u^{\max}$ is observed in $\mathcal{B} < 0.15$ cases compared to the HD flow, as shown in Fig. 3(b). Furthermore, it can be seen that with $\mathcal{B} \geqslant 0.25$, E_r declines to values lower than that in the corresponding HD counterpart, which causes the mixing intermittency levels to be decreased. These analogies can be observed by comparing the magnitudes of E_r at $(t = 25\tau)$ over the range of $\mathcal{B}$ [Fig. 4(a)] with $S_u^{\max}$ [Fig. 3(b)].

The above results clearly show that the intensity of initial magnetic field plays a significant role in mixing layer intermittency due to its influence on E_r. Furthermore, study of the Reynolds number ratio ($\mathrm{Re}_r = \mathrm{Re}_H/\mathrm{Re}_L$) allows the impact of the magnetic field to be evaluated on both turbulent kinetic energy and the length scale ratio.

Figure 4(b) shows the evolution of Re_r over the range of $\mathcal{B}$. It can be observed that there is a close agreement between the magnitudes of $\mathrm{Re}_{r(t=25\tau)}$ at different magnetic field intensities [Fig. 4(b)] and $S_u^{\max}$ in Fig. 3(b). It can be seen that, similar to $S_u^{\max}$, the values of $\mathrm{Re}_{r(t=25\tau)}$ with $\mathcal{B} \leqslant 0.15$ are larger than HD counterpart. Moreover, increasing $\mathcal{B}$ leads to decrease in $\mathrm{Re}_{r(t=25\tau)}$ such that its value with $\mathcal{B} \geqslant 0.25$ is lower than that in its counterpart HD simulation. This demonstrates that the variations of the Reynolds number ratio are a proper indicator for the intermittency variations. It should be noted that, since the kinematic viscosity is the same in both $\mathrm{HIT_H}$ and $\mathrm{HIT_L}$, Re_r represents only the variations of ℓ_r and square root of E_r.

Since behaviors of all $S_u^{\max}$, E_r, and Re_r parameters are related to variations of the velocity field by the Lorentz force, the interaction of the velocity and magnetic field is also investigated. In the MHD flow with imposed initial random seed magnetic field, the random stretching of the magnetic lines by the velocity field tends to increase the induced magnetic field, $\vec{b}$, and consequently the magnetic energy $\langle b^2 \rangle$ [16]. On the other hand, increasing $\vec{b}$ results in suppression of velocity field and turbulent kinetic energy through the Lorentz force. It can be interpreted that energy transfers from the flow field to magnetic field by a common term of $(\vec{u} \cdot (\vec{J} \times \vec{b}))$ in both kinetic and magnetic energy equations [16]. Eventually, the transferred energy is converted to heat through Ohmic dissipation.

Accordingly, to compare the capability of Lorentz force (which transfers the kinetic energy to the magnetic field) with the inertial force (which is responsible for energy transfer from the high- to low-energy regions), the dimensionless parameter ξ is defined as

$$\xi = \frac{\text{Lorentz force}}{\text{Inertial force}} = \frac{\langle |\vec{J} \times \vec{b}| \rangle}{\langle |(\vec{u} \cdot \vec{\nabla})\vec{u}| \rangle}. \tag{19}$$

This parameter is identical to the interaction parameter where the low magnetic Reynolds number flows with the imposed external magnetic field are considered [16].

Figures 5(a) and 5(b) show the time evolution of ξ in $\mathrm{HIT_L}$ (ξ_L) and $\mathrm{HIT_H}$ (ξ_H), respectively. It is clearly observed that both ξ_L and ξ_H decline, which means that the impact of the magnetic field on flow field is reduced over time. In Fig. 5(a), it can be observed that the values ξ_L are larger than one for all values of $\mathcal{B}$, which signifies the higher quantity of Lorentz force compared to inertial force. This causes the velocity field in $\mathrm{HIT_L}$ to be rapidly suppressed, and hence, the turbulent kinetic energy is decreased. In contrast, in Fig. 5(b), ξ_H for $\mathcal{B} < 0.15$ is always below one and for $\mathcal{B} \geqslant 0.25$ is above one.

By comparing ξ_H and ξ_L with Figs. 4(a) and 4(b), it is observed that for the cases, in which $\xi_L > 1$ and $\xi_H < 1$ (i.e., $\mathcal{B} = 0.05$), the ratio of suppressed kinetic energy by the Lorentz force to the energy transferred in the mixing layer by the convection term is greater in $\mathrm{HIT_L}$ compared to $\mathrm{HIT_H}$. In this situation, E_r and Re_r are increased, which results in enhancement of intermittency [see Figs. 3(b), 4(a), and 4(b)]. Whereas, in the cases where both ξ_H and ξ_L are larger than 1 ($\mathcal{B} = 0.25$ and 0.5), the rates of energy suppression in both HIT regions are in such a way that E_r and Re_r reduce. An analogy between variations of Re_r [Fig. 4(b)] and ξ [Figs. 5(a) and 5(b)] for $\mathcal{B} = 0.15$, in which the ξ_H in the transient period ($\tau < 5$) is higher than 1 and in the developed stage ($\tau > 5$) is less than one, also matches the above results' description.

B. Effect of magnetic field on mixing efficiency and thickness layer growth

In this section, the impacts of the variation of the initial magnetic field on the mixing efficiency and the thickness growth of the mixing layer are evaluated. It is commonly believed that vortex stretching is responsible for the turbulent

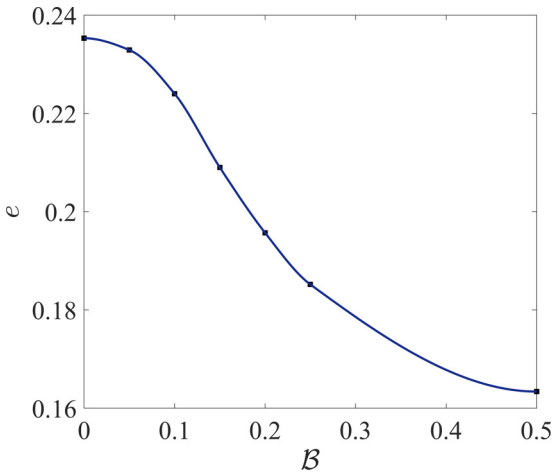

FIG. 6. The time-averaged mixing efficiency at the well-developed stage ($t > 10\tau$) as a function of $\mathcal{B}$.

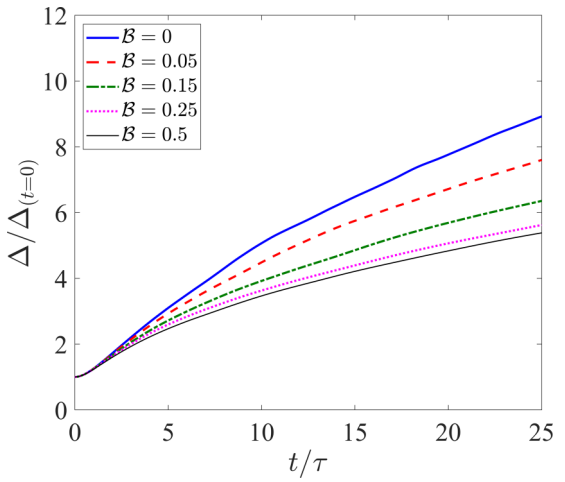

FIG. 7. Time evolution of the normalized mixing layer thickness for different intensities of $\mathcal{B}$.

mixing. Indeed, in 2D flows there is no vortex stretching. However, the extension of the material lines and hence the isovortical lines leads to deforming the vorticity blobs to fine-scale structures and vorticity filaments [37]. These vorticity filaments produce and control the strain field and therefore cause the turbulent mixing [44].

In order to quantify the above mentioned process, the mixing efficiency of the flow field (e) is investigated based on the normalized material line growth,

$$e = \frac{1}{\Delta(t)} \int_{\Delta(t)} \overline{\left(\frac{l_i l_j s_{ij}}{\sqrt{s_{ij} s_{ij}}} \right)} dx, \tag{20}$$

where $l_i = dx_i/|dx_i|$ is the direction vector of the material line $|dx|$, and $s_{ij} = (\partial_j u_i + \partial_i u_j)/2$ is the strain rate tensor [1,5]. It can be proven that, in the incompressible 2D flow, Eq. (20) is simplified to $(\sqrt{2}/2)\overline{\cos(2\alpha)}$, where α is the angle between the l_i and the compressing eigenvector of the strain rate tensor [44].

Figure 6 shows the time-averaged mixing efficiency at the well-developed stage ($t > 10\tau$) as a function of $\mathcal{B}$. This figure illustrates the reduction of mixing efficiency by increasing $\mathcal{B}$. The mixing efficiency is attributed to sporadic penetration of energetic eddies into the mixing layer, which leads to flow field agitation of the mixing region [5]. Therefore, the results of the mixing efficiency indicate the decay of random motion of flow fields and frequent penetration of energetic eddies into the mixing layer, due to the increase of $\mathcal{B}$. The reduction of sporadic penetration of energetic eddies also affects the growth of mixing layer thickness, which is another parameter for evaluation of the mixing progress. This thickness represents the extent of penetration of passive scalars from one HIT region into the adjacent HIT region, which is employed as an indicator of the mixing layer growth.

Figure 7 displays the time evolution of the mixing layer thickness normalized by the initial thickness ($\Delta_{(t=0)}$) for different magnetic intensities. It is observed that the growth rate of mixing layer thickness decreases by increasing $\mathcal{B}$. This behavior is such that the thickness of the mixing layer in the hydrodynamic flow is about 1.5 times larger than its corresponding thickness in $\mathcal{B} = 0.5$, at the end of the simulation ($t = 25\tau$).

It should be noted that the influential parameters on the mixing efficiency and mixing layer thickness (i.e., agitation of flow field and random motion of energetic eddies into the mixing layer) are closely related to the Reynolds number of the HIT regions. Increasing the Reynolds number in both HIT regions enhances the random motion of flow fields as well as the frequent penetration of eddies into the mixing layer [5]. Therefore, to analyze the behaviors of the mixing efficiency and mixing layer thickness, the average of both HIT Reynolds numbers ($\mathrm{Re}^{\mathrm{ave}}$) is examined.

Figure 8 shows the temporal evolution of $\mathrm{Re}^{\mathrm{ave}}$ for different intensities of $\mathcal{B}$. It is observed that $\mathrm{Re}^{\mathrm{ave}}$ in hydrodynamic flow experiences a monotonic rise. In contrast, in all MHD cases, $\mathrm{Re}^{\mathrm{ave}}$ changes slightly after a sharp drop in the transient period ($\tau < 5$). Furthermore, the reduction of $\mathrm{Re}^{\mathrm{ave}}$ by increasing $\mathcal{B}$ is clearly observed over time, which is closely analogous to the trends of mixing efficiency and mixing layer thickness. This behavior is predictable because of velocity suppression in both HIT regions with the Lorentz

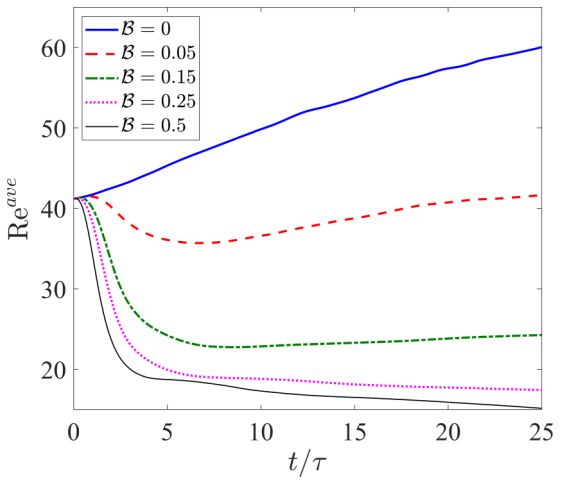

FIG. 8. Time evolution of the averaged Reynolds number for intensities of $\mathcal{B}$.

force, leading to a decrease of both Re_H and Re_L, and hence $\mathrm{Re}^{\mathrm{ave}}$.

IV. CONCLUSION

In this research, the effect of initial magnetic field intensity on the mixing characteristics of 2D incompressible turbulent shearless mixing layers is investigated using DNS. Different intensities of initial random seed magnetic field (with uniform probability distribution) are imposed on an identical flow field. The initial flow field is considered as the turbulent shearless mixing layer of two HIT regions with different kinetic energies and identical integral length scales. In this research the impact of different intensity of the initial magnetic field on the evolution of the flow field intermittency, thickness layer growth, and mixing efficiency is investigated.

The mixing layer intermittency of both large and small scales is measured by maximum values of velocity skewness and velocity derivative skewness, respectively. It is observed that in the MHD flows, both large- and small-scale intermittency are reduced by increasing the initial magnetic field intensity, $\mathcal{B}$. However, with small initial magnetic fields $\mathcal{B} \leqslant 0.15$, the mixing layer intermittency of both small and large scales is larger compared to those in the hydrodynamic flow. It is observed that in $\mathcal{B} \leqslant 0.15$, due to the suppressive effect of the Lorentz force on the flow field evolution, the turbulent kinetic energy in the low-energy region decays much faster than that in high energy region. This process results in the increase of the Reynolds number ratio. In cases with larger magnetic field intensities, the velocity field suppression rate in the high-energy region is more than that in the low-energy region. This leads to a reduction the Reynolds number ratio and consequently the flow field intermittency compared to the counterpart hydrodynamic flow.

Moreover, it is observed that increasing the initial magnetic field intensity has a hampering effect on the mixing efficiency and the growth of mixing layer thickness.

[1] J. M. Ottino, *The Kinematics of Mixing: Stretching, Chaos, and Transport*, Vol. 3 (Cambridge University Press, Cambridge, 1989).

[2] D. Tordella, M. Iovieno, and P. R. Bailey, Sufficient condition for Gaussian departure in turbulence, Phys. Rev. E **77**, 016309 (2008).

[3] B. Gilbert, Diffusion mixing in grid turbulence without mean shear, J. Fluid Mech. **100**, 349 (1980).

[4] S. Veeravalli and Z. Warhaft, The shearless turbulence mixing layer, J. Fluid Mech. **207**, 191 (1989).

[5] M. Fathali and M. K. Deshiri, Sensitivity of the two-dimensional shearless mixing layer to the initial turbulent kinetic energy and integral length scale, Phys. Rev. E **93**, 043122 (2016).

[6] D. Tordella and M. Iovieno, Numerical experiments on the intermediate asymptotics of shear-free turbulent transport and diffusion, J. Fluid Mech. **549**, 429 (2006).

[7] D. Tordella and M. Iovieno, Decaying turbulence: What happens when the correlation length varies spatially in two adjacent zones, Physica D **241**, 178 (2012).

[8] H. S. Kang and C. Meneveau, Experimental study of an active grid-generated shearless mixing layer and comparisons with large-eddy simulation, Phys. Fluids **20**, 125102 (2008).

[9] D. Tordella and M. Iovieno, Small-Scale Anisotropy in Turbulent Shearless Mixing, Phys. Rev. Lett. **107**, 194501 (2011).

[10] M. Iovieno, S. Di Savino, L. Gallana, and D. Tordella, Mixing of a passive scalar across a thin shearless layer: Concentration of intermittency on the sides of the turbulent interface, J. Turbul. **15**, 311 (2014).

[11] P. E. Dimotakis, Turbulent mixing, Annu. Rev. Fluid Mech. **37**, 329 (2005).

[12] P. Götzfried, B. Kumar, R. A. Shaw, and J. Schumacher, Droplet dynamics and fine-scale structure in a shearless turbulent mixing layer with phase changes, J. Fluid Mech. **814**, 452 (2017).

[13] G. Cocconi, E. De Angelis, B. Frohnapfel, M. Baevsky, and A. Liberzon, Small scale dynamics of a shearless turbulent/non-turbulent interface in dilute polymer solutions, Phys. Fluids **29**, 075102 (2017).

[14] A. F. Samer and M. Epaminondas, Spark ignition of a turbulent shear-less fuel–air mixing layer, Fuel **164**, 297 (2016).

[15] E. M. AttarZade, S. Tabejamaat, M. Mani, and M. Farshchi, Numerical study of ignition process in turbulent shear-less methane-air mixing layer, Flow, Turbul. Combust. **99**, 411 (2017).

[16] P. A. Davidson, *An Introduction to Magnetohydrodynamics*, Cambridge Texts in Applied Mathematics (Cambridge University Press, Cambridge, 2001).

[17] W. Horton, T. Tajima, and T. Kamimura, Kelvin–Helmholtz instability and vortices in magnetized plasma, Phys. Fluids **30**, 3485 (1987).

[18] T. Nakamura, H. Hasegawa, and I. Shinohara, Kinetic effects on the Kelvin–Helmholtz instability in ion-to-magnetohydrodynamic scale transverse velocity shear layers: Particle simulations, Phys. Plasmas **17**, 042119 (2010).

[19] A. Frank, T. Jones, D. Ryu, and J. B. Gaalaas, The MHD kelvin-helmholtz instability: A two-dimensional numerical study, Astrophys. J. **460**, 777 (1996).

[20] M. Fujimoto and T. Terasawa, Anomalous ion mixing within an MHD scale Kelvin-Helmholtz vortex, J. Geophys. Res.: Space Phys. **99**, 8601 (1994).

[21] M. Fujimoto and T. Terasawa, Anomalous ion mixing within an MHD scale Kelvin-Helmholtz vortex: 2. Effects of inhomogeneity, J. Geophys. Res.: Space Phys. **100**, 12025 (1995).

[22] T. K. M. Nakamura, M. Fujimoto, and A. Otto, Structure of an MHD-scale Kelvin-Helmholtz vortex: Two-dimensional two-fluid simulations including finite electron inertial effects, J. Geophys. Res.: Space Phys. **113**, A09204 (2008).

[23] T. K. M. Nakamura, H. Hasegawa, I. Shinohara, and M. Fujimoto, Evolution of an MHD-scale Kelvin-Helmholtz vortex accompanied by magnetic reconnection: Two-dimensional particle simulations, J. Geophys. Res.: Space Phys. **116**, A03227 (2011).

[24] S. C. Kassinos, B. Knaepen, and D. Carati, The transport of a passive scalar in magnetohydrodynamic turbulence subjected to mean shear and frame rotation, Phys. Fluids **19**, 015105 (2007).
[25] G. Rezgui, H. Marzougui, and T. Lili, Passive scalar evolution in sheared homogeneous magnetohydrodynamic turbulence, Phys. Plasmas **24**, 102309 (2017).
[26] X. Xu, D. Rouson, S. C. Kassinos, and H. Radhakrishnan, Dispersed-phase structure in sheared MHD turbulence, J. Turbul. **13**, 1 (2012).
[27] O. Debliquy, B. Knaepen, and D. Carati, Large-eddy simulation of a shear-free magnetohydrodynamic mixing layer, Technical report, Université Libre de Bruxelles, Belgium, Statistical and Plasma Physics (2001).
[28] A. A. Chernyshov, K. V. Karelsky, and A. S. Petrosyan, Validation of large eddy simulation method for study of flatness and skewness of decaying compressible magnetohydrodynamic turbulence, Theor. Comput. Fluid Dyn. **23**, 451 (2009).
[29] A. Lazarian, Intermittency of magnetohydrodynamic turbulence: Astrophysical perspective, Int. J. Mod. Phys. D **15**, 1099 (2006).
[30] M. K. Verma, Statistical theory of magnetohydrodynamic turbulence: Recent results, Phys. Rep. **401**, 229 (2004).
[31] D. Biskamp, *Magnetohydrodynamic Turbulence* (Cambridge University Press, Cambridge, 2003).
[32] R. H. Kraichnan, Inertial range spectrum of hydromagnetic turbulence, Phys. Fluids **8**, 1385 (1965).
[33] M. K. Verma, Mean magnetic field renormalization and Kolmogorov's energy spectrum in magnetohydrodynamic turbulence, Phys. Plasmas **6**, 1455 (1999).
[34] B. Knaepen, O. Debliquy, and D. Carati, Direct numerical simulation and large-eddy simulation of a shear-free mixing layer, J. Fluid Mech. **514**, 153 (2004).
[35] J. Chasnov, On the decay of two-dimensional homogeneous turbulence, Phys. Fluids **9**, 171 (1997).
[36] A. Lowe and P. Davidson, The evolution of freely-decaying, isotropic, two-dimensional turbulence, Eur. J. Mech. B-Fluids **24**, 314 (2005).
[37] P. Davidson, *Turbulence: An Introduction for Scientists and Engineers* (Oxford University Press, Oxford, 2015).
[38] A. S. Monin and A. M. Yaglom, *Statistical Fluid Mechanics, Vol. II: Mechanics of Turbulence* Vol. 2 (Dover Publications, New York, 2013).
[39] P. A. Davidson, *Turbulence in Rotating, Stratified and Electrically Conducting Fluids* (Cambridge University Press, Cambridge, 2013).
[40] A. Brandenburg and K. Subramanian, Astrophysical magnetic fields and nonlinear dynamo theory, Phys. Rep. **417**, 1 (2005).
[41] O. Debliquy, M. K. Verma, and D. Carati, Energy fluxes and shell-to-shell transfers in three-dimensional decaying magnetohydrodynamic turbulence, Phys. Plasmas **12**, 042309 (2005).
[42] D. G. Fox and S. A. Orszag, Pseudospectral approximation to two-dimensional turbulence, J. Comput. Phys. **11**, 612 (1973).
[43] S. B. Pope, *Turbulent Flows* (Cambridge University Press, Cambridge, 2000).
[44] B. Protas, A. Babiano, and N.-R. Kevlahan, On geometrical alignment properties of two-dimensional forced turbulence, Physica D **128**, 169 (1999).